TECHNICAL MEMORANDUM

44

In the mass balance correction in diagnostics studies

H. Sävijärvi

Research Department

November 1981

European Centre for Medium-Range Weather Forecasts
Europäisches Zentrum für mittelfristige Wettervorhersage
Centre européen pour les prévisions météorologiques à moyen

1. INTRODUCTION

In most diagnostic studies the large-scale non-observed vertical velocity component of air is needed. The most common way to estimate this small but important variable has been the kinematic method, whereby, using the continuity equation in pressure coordinates

$$\frac{\partial \omega}{\partial p} = - \nabla_p \cdot \underline{v}$$

the horizontal wind divergence, estimated from observed winds at some pressure levels, is integrated from top to bottom starting from a boundary value ω_T; for instance setting $\omega_T = 0$ at some stratospheric level. It is typical, however, at least with aerological wind data that if the integration is done through a considerable depth of a vertical column the resulting ω_B is far from zero even for time-averaged winds. This means that the time mean mass balance in the column is incorrect, physically indicating mass divergence or convergence to the column through horizontal boundaries. This false mass convergence must be removed if the diagnostics is to have any credibility. Various schemes to distribute the correction in vertical have been suggested on an ad hoc basis; O'Brien (1970) has reviewed the problem (which from the mathematical point of view is the overspecification of first-order differential equation with two boundary conditions) and suggested that the mass balance correction be divided linearly in pressure. Fig. 1 shows schematically a divergence profile and two common ways of mass balance correction.

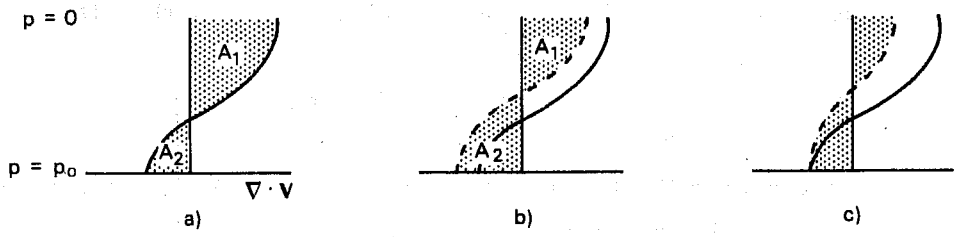

Fig. 1 a) Schematic structure of a typical "observed" time mean large scale divergence profile with false mass balance; $A_1 \neq A_2$.
b) Divergence profile with mass balance correction constant in pressure.
c) Divergence profile with mass balance correction linear in pressure. Note that the shape of the profile is modified.

Apart from these explicit correction methods some studies (e.g. Perry, 1967, Savijärvi, 1977) have implicitly forced the mass balance by fitting an analytic curve to the observed divergences with constraints that set ω_T and ω_B to predescribed values in the analytic integration of the curve.

In this report the mass balance problem is discussed in the σ-coordinate system. An example of σ-coordinate calculations is given in the form of the area and time-averaged sensible heat budget, which is sensitive to local mass imbalance, from ECMWF initialized analysis and from ECMWF forecasts. The initialized analyses have a negligible local mass imbalance while the spatially variable time-increasing systematic error of the numerical model appears as local mass imbalance in the forecast data.

This work is based on the one year data used in a more detailed study of limited area energy budgets (Savijärvi, 1981).

2. MASS BALANCE EFFECTS IN THE σ-COORDINATE SYSTEM

Because the vertical boundary conditions are easy to include in σ-coordinates, we use this vertical coordinate system. Here $\sigma = p/p_s$ is pressure normalized by the surface pressure. A generalization to pressure coordinates is straightforward provided that the variable lower boundary $p_s(\lambda,\phi,t)$ is handled appropriately. The governing equations in the σ-system are based on the pressure system equations and are thus assuming hydrostatic balance. The equation of continuity for a unit mass of air is (e.g. Holton, 1980):

$$\frac{\partial p_s}{\partial t} = -\nabla_\sigma \cdot (p_s \underline{v}) - \frac{\partial}{\partial \sigma}(p_s \dot{\sigma}) \qquad (1)$$

The most often used vertical boundary conditions are that the air cannot penetrate through the top and bottom surfaces ("closed lids"), that is:

$$\dot{\sigma} = \frac{d\sigma}{dt} = 0 \text{ at } \sigma = 0 \ (p = 0) \text{ and at } \sigma = 1 \ (p = p_s) \qquad (2)$$

If (1) is integrated vertically through the atmosphere from $\sigma = 0$ to $\sigma = 1$ and the boundary conditions (2) are applied, we get

$$\frac{\partial p_s}{\partial t} = -\int_0^1 \nabla_\sigma \cdot (p_s \underline{v}) \, d\sigma \qquad (3)$$

By equating (1) and (3) it can be seen that at each level the 3-dimensional mass flux convergence must be equal to the vertical average of the horizontal flux convergence only. Using this fact (integrating (1) from 0 to σ and applying both (2) and (3)) gives the diagnostic equation by which $p_s\dot{\sigma}$ is calculated, e.g. in numerical σ-coordinate models:

$$p_s \dot{\sigma} = - \int_0^{\sigma} \nabla_\sigma \cdot (p_s \underline{v}) \, d\sigma + \sigma \int_0^1 \nabla_\sigma \cdot (p_s \underline{v}) \, d\sigma \qquad (4)$$

If the equations (1) - (4) are time-averaged over a long period, denoting time averages by an overbar, the time mean local surface pressure change $\partial \bar{p}_s / \partial t$ should become small at any point. According to (3) the time and vertically averaged horizontal mass flux convergence $- \int_0^1 \nabla_\sigma \cdot (\overline{p_s \underline{v}}) \, d\sigma$ must then vanish in any air column.

However, if observed horizontal winds are used to estimate the time mean mass flux $\overline{p_s \underline{v}}$, the integrated horizontal mass flux convergence does not normally vanish. The implied non-vanishing local surface pressure change, which accounted to 18 mb/day over Europe in recent 3-year aerological data material (Alestalo, 1981), must be corrected. Define the correction a as the error in the observed horizontal mass flux convergence at each level:

$$a = - \nabla \cdot (\overline{p_s \underline{v}})_{true} - (- \nabla \cdot (\overline{p_s \underline{v}})_{obs}) \qquad (5)$$

then

$$\hat{a} = \int_0^1 a \, d\sigma = \int_0^1 \nabla \cdot (\overline{p_s \underline{v}})_{obs} \, d\sigma = - \partial \bar{p}_s / \partial t$$

Because the vertical boundary conditions are valid also in the time-averaged data, the vertical variation of a around its mean value $\hat{a}$ is associated with the error structure in the vertical mass convergence in σ-system. If $a(\sigma)$ is kept constant (in analogue to Fig. 1b), no error at all is assumed in the "observed" vertical convergence while linear variation (Fig. 1c) implies no error in midtroposphere. The choice must depend on data quality.

The horizontal convergence of the time mean flux of any scalar variable f is in σ-coordinate system:

$$- \nabla_\sigma \cdot (\overline{f p_s \underline{v}}) = - \bar{f} \nabla \cdot (\overline{p_s \underline{v}}) - \overline{p_s \underline{v}} \cdot \nabla \bar{f} - \nabla \cdot \overline{f' (p_s \underline{v})'} \qquad (6)$$

Using (5) to correct the time-mean observed mass flux convergence in (6) gives a better estimate for the f-flux convergence:

$$- \nabla \cdot (\overline{f p_s \underline{v}})_{true} \cong - \nabla \cdot (\overline{f p_s \underline{v}})_{obs} + \bar{f}_{obs} \; a \qquad (7)$$

For the 3-dimensional flux convergence the correction is $\bar{f}_{obs} \cdot \hat{a}$, thus following the profile of $\bar{f}(\sigma)$. The mass balance correction is only important if the mean divergent part of (6) is dominant. This is the case for the sensible

heat and geopotential fluxes but, fortunately, not for kinetic energy or latent heat energy flux.

The flux form of the time mean sensible heat budget is in σ-coordinates

$$\frac{\partial}{\partial t}(c_p \overline{p_s T}) = - \nabla_\sigma \cdot (c_p \overline{T p_s \underline{v}}) - \frac{\partial}{\partial \sigma} (c_p \overline{T p_s \dot{\sigma}}) + \overline{p_s \alpha \omega} + \overline{p_s Q} \qquad (8)$$

The correction for the "observed" 3-dimensional convergence is $c_p \bar{T} \cdot \int_0^1 \nabla \cdot (\overline{p_s \underline{v}})\, d\sigma$; this of course formally balances the mean local change part $c_p \bar{T} \cdot (\frac{\partial \bar{p}_s}{\partial t})$ on the left hand side.

The extra mass convergence, if it exists, is also present in the αω-term, because ω in the σ-levels is given by

$$\omega = \frac{d}{dt} (p_s \sigma) = p_s \dot{\sigma} + \sigma \, (\frac{\partial p_s}{\partial t} + \underline{v} \cdot \nabla p_s) \qquad (9)$$

and, using (3) and (4):

$$p_s \, \alpha\omega = p_s \frac{RT}{p} \omega = RT \, \underline{v} \cdot \nabla p_s - \frac{RT}{\sigma} \int_0^\sigma \nabla_\sigma \cdot (p_s \underline{v}) \, d\sigma \qquad (10)$$

After time averaging and correcting the time-mean part of the last term in (10) by using (5), we get an estimate for the "true" $\overline{p_s \alpha\omega}$:

$$(\overline{p_s \alpha\omega})_{true} \cong (\overline{p_s \alpha\omega})_{obs} + \frac{\overline{RT}}{\sigma} \cdot \int_0^\sigma a \, d\sigma \qquad (11)$$

Thus it can be expected that for the conversion term the mass balance correction appears proportional to temperature and is roughly $R/c_p = 0.286$ of the correction $c_p \bar{T}.a$ needed for the temperature flux convergence, if the mass balance error is nearly evenly distributed in σ and it is the major error source in the observed $\overline{p_s \alpha\omega}$.

Considering the geopotential flux convergence, which is important in the atmospheric total energy balance, we first write the diagnostic relation between the kinetic energy generation, pressure forces and energy conversion in σ-coordinates, which must be valid at all times:

$$\underset{\text{(kinetic energy generation)}}{-p_s \underline{v} . \nabla \phi - RT \underline{v} . \nabla p_s} + \underset{\text{(pressure force)}}{\nabla_\sigma . (\phi p_s \underline{v}) + \frac{\partial}{\partial \sigma} (\phi p_s \dot{\sigma} + \phi \sigma \frac{\partial p_s}{\partial t})} + \underset{\text{(conversion)}}{p_s \alpha\omega} = 0 \qquad (12)$$

For the time-averaged 3-dimensional divergence of geopotential flux (the horizontal divergence plus first part of the vertical divergence term in (12)) the correction is $-\bar{\phi}\, \hat{a}$, according to (7). The second part of the vertical

divergence term can be rewritten as

$$\frac{\partial}{\partial\sigma}\left(\phi\sigma\frac{\partial p_s}{\partial t}\right) = \sigma\frac{\partial}{\partial\sigma}\left(\phi\frac{\partial p_s}{\partial t}\right) + \phi\frac{\partial p_s}{\partial t} = -RT\frac{\partial p_s}{\partial t} + \phi\frac{\partial p_s}{\partial t} \qquad (13)$$

and so must have a correction of $-R\overline{T}\,\hat{a} + \overline{\phi}\hat{a}$ in the time mean. For the pressure forces the correction is thus $-\overline{RT}\,.\,\hat{a}$, and not $-\overline{\phi}.\hat{a}$, because of the important extra term (13), which in the pressure coordinate system is hidden into the variable lower boundary conditions.

The errors in $p_s\alpha\omega$ and pressure forces cancel except for the integrated vertical variation of the error in the conversion term leaving the kinetic energy generation (the first two terms in (12)) to be relatively accurately determined from data, in spite of the fact that this term is dependent mainly on the divergent part of the wind.

3. SENSIBLE HEAT BUDGET OVER NORTH AMERICA

Since November 1979 the daily budgets of kinetic energy, sensible heat and latent heat energy have been diagnosed over several limited areas in ECMWF using the ECMWF initialized grid point σ-level analyses and 15-level model forecasts as data. Detailed results for one year have been reported in Savijärvi (1981); what follows is a closer examination of the mass balance in the forecast data.

The area selected here for demonstration of the sensible heat budget is continental North America within latitudes 30 - 70°N and longitudes 80°W - 140°W. This area is within good aerological data network, and the kinetic energy budget from the ECMWF analyzed data was rather similar to 5-year aerological data studies for the same area by Kung et al (1967, 1975). Also the temperature budget agreed in general to the few earlier studies (e.g. Lau (1979), Savijärvi (1977), for wintertime circulation).

The temperature budget in the calculations is the second-order finite difference equivalence of Eqns. (8) and (10) in the staggered Arakawa C-scheme grid. The objectively analyzed data has been initialized with the adiabatic nonlinear normal mode method (Temperton and Williamson, 1979). Resolution in the calculations is $\Delta\lambda = \Delta\theta = 1.875°$, and 15 levels in σ.

The finite difference scheme follows closely that of the ECMWF grid point model. Equivalently with the model, the diagnostic relation (12) is accurate (no computational residual). As discussed in Burridge (1979) this requires that α in the energy conversion term $p_s\alpha\omega$ is consistent with the numerical formulation

of the hydrostatic equation; here

$$p\alpha = RT = -\Delta_\sigma \phi / \Delta_\sigma \ln \sigma \qquad (14)$$

was used (cf, Hollingsworth et al, 1980) to give ϕ from temperature without virtual correction.

Fig. 2 shows the one year time mean (December 1979 - November 1980) of the sensible heat budget (Eqn. (8) divided by g to give the convenient unit W/m^2) over the North American area, from all 12 GMT ECMWF initialized analyses (355 cases). The most obvious feature in Fig. 2 is the strong compensation between the horizontal and vertical flux convergences (due to the dominance of the divergent part in the temperature flux) adding up to total temperature flux divergence, which is largely compensated by adiabatic heating in sinking motion through the positive $\overline{p_s \alpha \omega}$-term. Because the local change term disappears for one year time mean in the analyzed data (disregarding diurnal variation), the residual needed to balance Eqn. (8) is an estimate of the net diabatic heating; positive near the ground and weakly negative in the free troposphere.

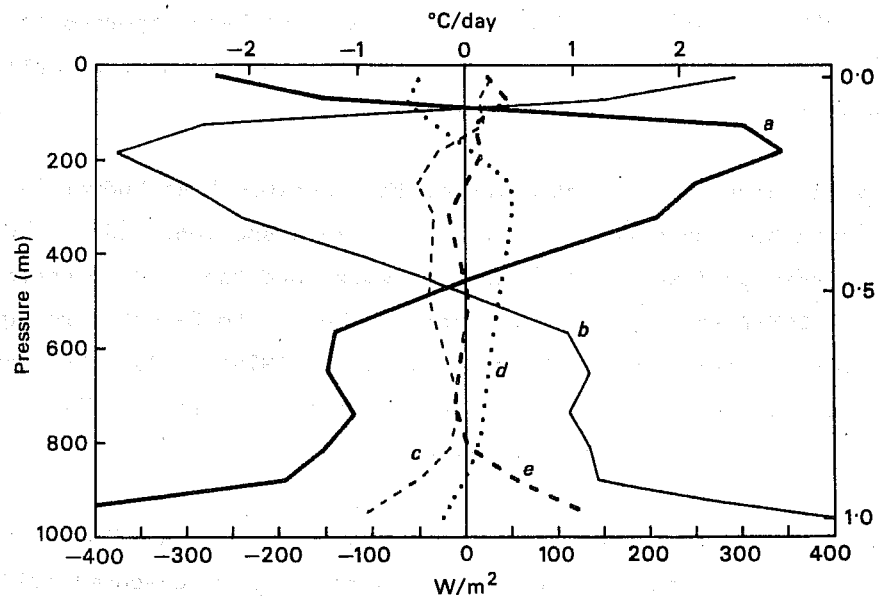

Fig. 2 The time and area-averaged sensible heat budget over North America (80-140°W, 30-70°N) from ECMWF initialized 12 GMT analyses during December 1979 - November 1980. Unit: W/m^2.

a) horizontal flux convergence $-\nabla_\sigma \cdot (\overline{c_p T\, p_s \underline{V}})/g$

b) vertical flux convergence $-\frac{\partial}{\partial \sigma} (\overline{c_p T\, p_s \dot{\sigma}})/g$

c) 3-dimensional flux convergence (sum of a and b).

d) energy conversion $\overline{p_s \alpha \omega / g}$

e) estimate of diabatic heating, - (c+d)

If O GMT analyses are taken instead of 12 GMT, Fig. 2 is slightly different in numerical values. The migrating diurnal and semidiurnal thermal tidal effects in the observed data are, at least partly, surviving through the analysis-initialization scheme and create small but systematic diurnal winds, which trigger small local mass imbalances to the local temperature budget. To remove this we take the mean of results from four daily analyses at 0, 6, 12, 18 GMT.

Fig. 3 shows the resulting 3-dimensional temperature flux convergence and the adiabatic heating profiles from the analysed data for one year over North America taking 4 analyses per day (1414 cases). The same terms are also shown for the same area calculated and ensemble averaged from all available ECMWF 3-day forecasts (285 cases) within the year. Compared to the analysed results the profiles from the forecasts are shifted towards positive values. For the temperature flux convergence the shift analysis-forecast is about -110 W/m² for the conversion about -30 W/m², their relation 0.27 being near to R/c_p=0.286 as could be expected from the discussion in Section 2.

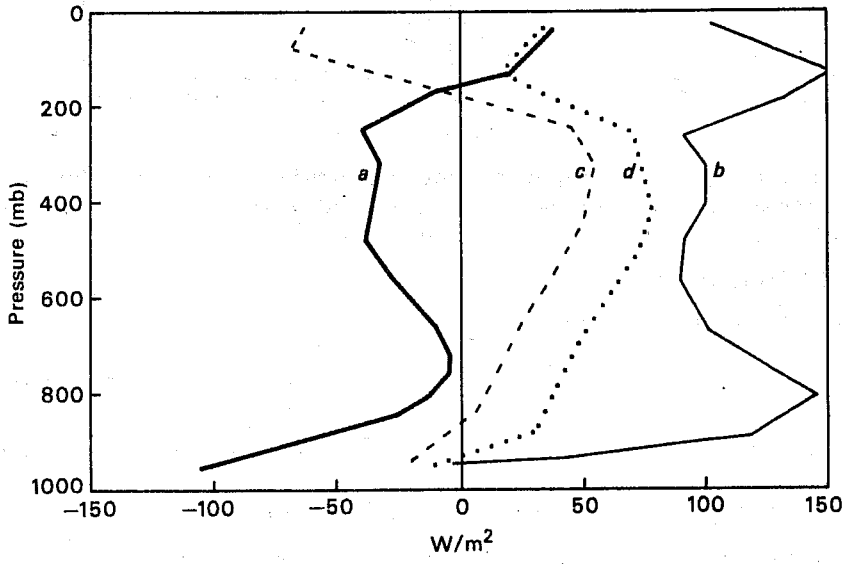

Fig. 3 The time and area averaged heat budget terms over North America from ECMWF analyses (4 per day) and forecasts for day 3 during December 1979 - November 1980. Unit: W/m².

a) 3-dimensional heat flux convergence from analysed data

b) 3-dimensional heat flux convergence from day 3 forecasts

c) energy conversion $\overline{p_s \alpha \omega / g}$ from analysed data

d) energy conversion $\overline{p_s \alpha \omega / g}$ from day 3 forecasts

Fig. 4 shows the individual energy conversion terms of Eqn. (12) calculated from analyses and day 3 forecasts. The vertically almost constant difference between $\alpha\omega$ calculated from forecasts and analyses is accompanied with similar but opposite shift in the pressure force, as discussed in Section 2. The kinetic energy generation term remains thus nearly the same in the analyzed and forecast data, except in the boundary layer. It is also very similar to independent calculations from aerological data (Kung, 1967).

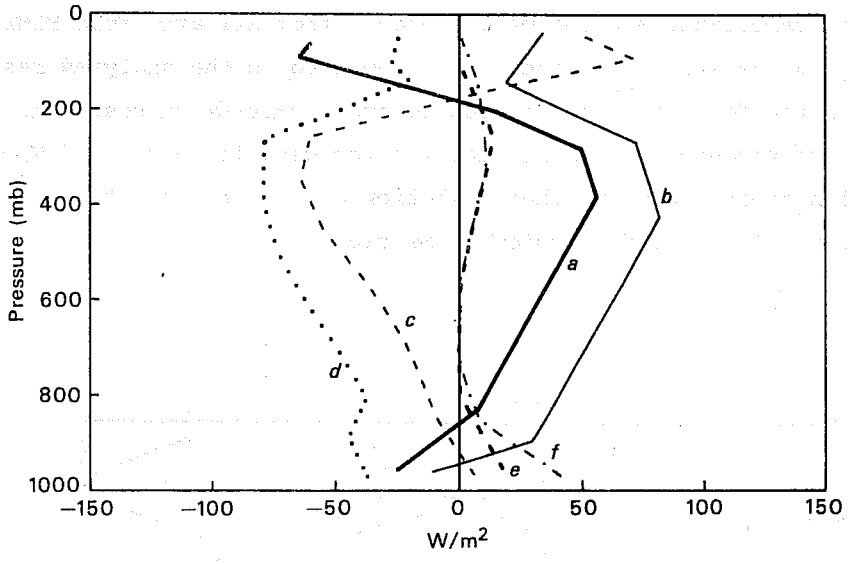

Fig. 4 The time and area averaged energy conversion terms over North America from ECMWF analyses (4 per day) and forecasts for day 3 during December 1979 - November 1980. Unit: W/m^2.

a) $\overline{p_s \alpha\omega/g}$ from analysed data

b) $\overline{p_s \alpha\omega/g}$ from day 3 forecasts

c) pressure forces $\nabla_\sigma \cdot (\overline{\phi p_s \underline{V}}) + \frac{\partial}{\partial\sigma}(\overline{\phi p_s \dot{\sigma}} + \overline{\phi\sigma \frac{\partial p_s}{\partial t}})$ from analysed data

d) pressure forces $\nabla_\sigma \cdot (\overline{\phi p_s \underline{V}} + \frac{\partial}{\partial\sigma}(\overline{\phi p_s \dot{\sigma}} + \overline{\phi\sigma \frac{\partial p_s}{\partial t}})$ from day 3 forecasts

e) kinetic energy generation from analysed data

f) kinetic energy generation from day 3 forecast data

If another area or forecast ensemble is chosen, the shift between forecast and analysed results varies (Figs. 3 and 4 are from a rather extreme case for a clearer illustration of the effect) but remains nearly constant in vertical. This shift is the outcome of the systematic error in the ECMWF model. The structure of the systematic error varies from month to month but is in general negative (forecast heights too low) over eastern Atlantic and Pacific, having basically the same horizontal pattern at all levels. From day 2 to day 4 the forecast 1000 mb heights are typically increasing over North America indicating surface pressure rise in this area. In longer 6-10 day forecasts the negative error pattern prevails also over the North American continent; this surface pressure drop is seen in the sensible heat budget as a shift to opposite direction of that in Figs. 3 and 4.

If the difference between the sensible heat budget terms calculated from forecast and analysed data in Figs. 3 and 4 is all due to the varying local mass balance triggered by the wind divergence related to the systematic error, the implied surface pressure increase is about 3 mb/day. This is a large but not unrealistic value for a single forecast time step data. Part of the difference is, however, coming from errors in the mean advective and transient effects.

The difference in the 3-dimensional temperature flux convergence between analysed and forecast data in Fig. 3 is plotted into Fig. 5, together with the difference (analysed-forecast) for the horizontal and vertical flux convergences separately. It is seen that the total (3-dimensional) flux convergence difference is nearly constant vertically in the troposphere. The dashed line gives theoretical mass balance correction curve (7) $c_p \overline{T} \cdot \hat{a}$, using the forecast $c_p \overline{T}$-profile and $\hat{a} = - \partial \overline{p}_s / \partial t = -3$ mb/day. The deviations of the difference around this profile are due to the forecast errors in the transient and mean advective parts (Eqn. 6) and are relatively small in troposphere. The stratospheric wind (and temperature) analyses were not very good at the early phase of ECMWF operations so comparisons to forecasts are not reliable.

The vertical mean of the difference in the vertical temperature flux divergence vanishes, as expected, but its structure is complicated. The horizontal difference is an estimate for the profile of $c_p \overline{T}(\sigma) \cdot a(\sigma)$ in this case.

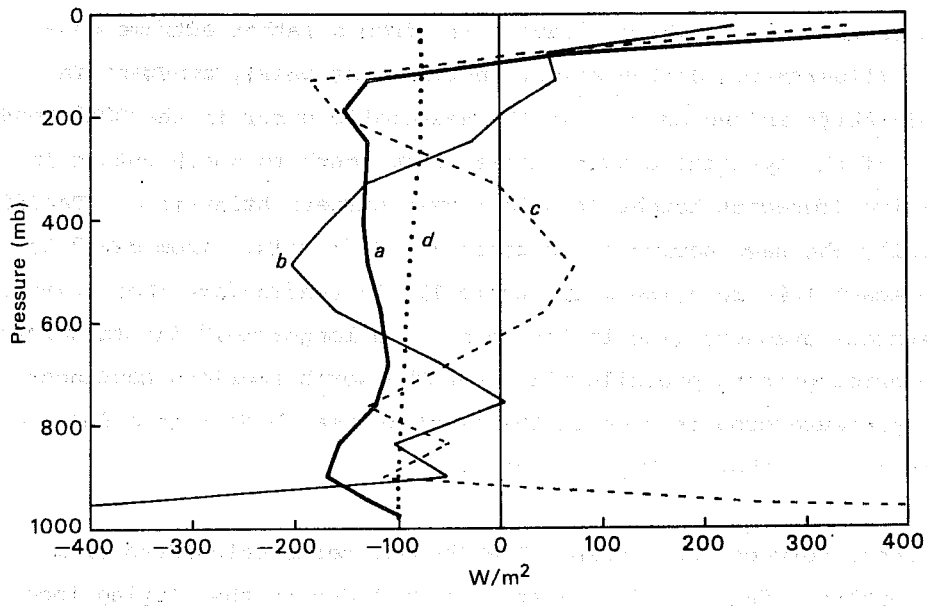

Fig. 5. The difference between analysed and forecast heat flux convergences over North America (from Fig. 3)

a) 3-dimensional flux convergence

b) horizontal flux convergence

c) vertical flux convergence

d) $c_p\bar{T} \cdot \hat{a}$ where $\hat{a} = -\partial\bar{p}_s/\partial t = -3$ mb/day

Fig. 6a gives the difference profiles (analysed-forecast) in the pressure force and $p_s\alpha\omega$. The difference profiles are nearly constant in troposphere. The even vertical distribution model of mass balance compensation $\pm R\bar{T} \cdot \hat{a}$ is given by the dashed lines in Fig. 6 and this is seen to be a good approximation in this case. For the horizontal and vertical pressure forces separately, Fig. 6b shows the difference profiles. Below 300 mb the respective theoretical distributions of even mass balance compensation, $-\bar{\phi}\,\hat{a}$ for the horizontal and $(\bar{\phi} - R\bar{T}) \cdot \hat{a}$ for the vertical term, are seen to explain the major part of the difference between the analysed and forecast geopotential flux divergences.

In practice normally the horizontal convergences of geopotential and temperature fluxes have to be corrected. Based on this data the geopotential flux convergence is not critical to the correction chosen while the temperature flux, rather unfortunately, is.

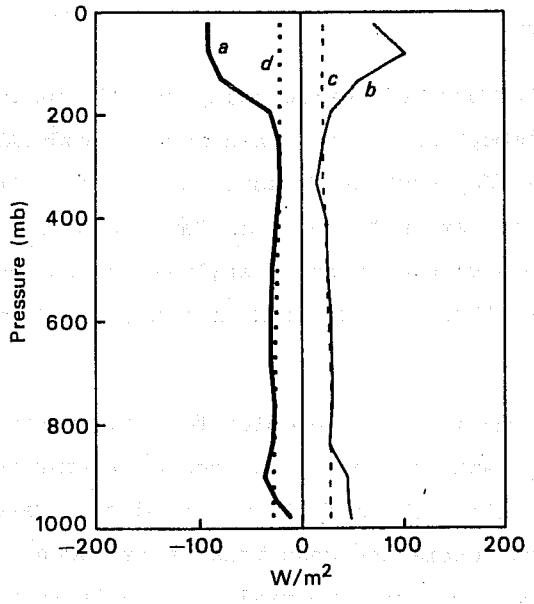

Fig. 6a) The difference between analysed and forecast pressure forces and conversion over North America (Fig. 4).

a) for energy conversion $\overline{p_s \alpha \omega}/g$

b) for pressure forces

c) $-R\bar{T} \cdot \hat{a}$ where $\hat{a} = -\partial\overline{p_s}/\partial t = -3$ mb/day

d) $+R\bar{T} \cdot \hat{a}$ where $\hat{a} = -\partial\overline{p_s}/\partial t = -3$ mb/day

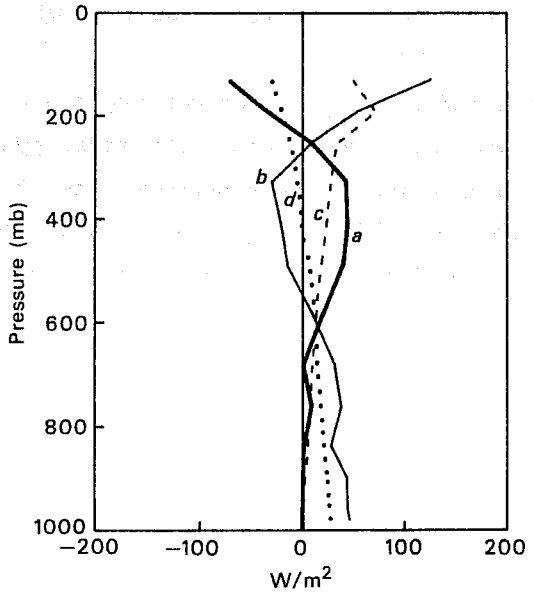

Fig. 6b) The difference between analysed and forecast horizontal and vertical pressure forces over North America

a) for horizontal forces $\nabla_\sigma \cdot (\overline{\phi p_s \underline{V}})/g$

b) for vertical forces $\frac{1}{g}\frac{\partial}{\partial\sigma}(\phi p_s \dot{\sigma} + \phi\sigma\frac{\partial p_s}{\partial t})$

c) $-\bar{\phi} \cdot \hat{a}$ where $\hat{a} = -\partial\bar{p}_s/\partial t = -3$ mb/day

d) $(\bar{\phi} - R\bar{T})\hat{a}$ where $\hat{a} = -\partial\bar{p}_s/\partial t = -3$ mb/day

5. CONCLUDING REMARKS

The "raw" aerological wind data do not normally fulfil the requirement of the local conservation of atmospheric mass; in a recent study Alestalo (1981) obtained a value of 18 mb/day surface pressure change over the continental Europe from 3 year good and large data material. In Savijärvi (1981) it was argued that the initialized ECMWF objective grid point analyses conserve the mass locally well and the analyses are thus suitable for localized diagnostic studies in this respect.

In the present paper the mass balance problem for diagnostic studies is discussed based on energy and mass conservationn equations on sigma (normalized pressure) levels. The deductions are demonstrated using the ECMWF model produced data, where the mass balance is known to be locally distorted due to the time-increasing spatially variable systematic error pattern of the model. The implied "mass balance correction" (forecast compared to the respective analysed values, which are assumed correct) is nearly constant in vertical and explains the major part of the difference between the forecast and analyzed sensible heat energy budget terms in the troposphere. The differences become very large in stratosphere but the analysis and forecast quality do not allow meaningful comparison there. In the boundary layer the ECMWF analysis is largely based on the 6 hour forecast background field and this prevents somewhat comparisons with the model.

The vertically even distribution of mass flux convergence error is in accordance with the barotropic nature of the ECMWF model systematic error (Derome, 1981). A similar systematic error pattern seems to be typical also for other short-range forecast models (Gadd, 1980), which are all based on hydrostatic equations and vanishing vertical boundary mass fluxes.

REFERENCES

Alestalo, M. 1981 The energy budget of the earth-atmosphere system in Europe. Tellus, 33, 360-371.

Burridge, D.M. 1979 Some aspects of large scale numerical modelling of the atmosphere. ECMWF Seminars on Dynamical meteorology and numerical weather prediction, Vol.2, 1-78.

Derome, J. 1981 On the average errors of an ensemble of forecasts. ECMWF Technical Report No.24.

Gadd, A. 1980 The GARP basic data set project. The experiment using GFDL analyses. GARP/WGNE Report No.20.

Holton, J. 1979 An introduction to dynamic meteorology. (2nd ed). Academic Press, pp.391.

Kung, E.C. 1967 Diurnal and long term variations of the kinetic energy generation and dissipation for a five-year period. Mon.Wea.Rev., 95, 593-606.

Kung, E.C. and Baker, W.E. 1975 Energy transformations in middle latitude disturbances. Quart.J.R.Met.Soc., 101, 793-815.

Lau, N.-C. 1979 The observed structure of tropospheric stationary waves and the local balances of vorticity and heat. J.Atm.Sci., 36, 996-1016.

O'Brien, J. 1970 Alternative solutions to the classical vertical velocity problem. J.Appl.Met., 9, 197-203.

Perry, J.S. 1967 Long wave energy processes in the 1963 sudden stratospheric warming. J.Atm.Sci., 27, 539-550.

Savijärvi, H. 1977 The interaction of the monthly mean flow and large-scale transient eddies in two different circulation types: Vorticity and temperature balance. Geophysica, 14, 207-229.

Savijärvi, H. 1981 The energy budgets in North America, North Atlantic and Europe based on ECMWF analysis and forecasts. ECMWF Technical Report No.27.